Dynamical conductivity of a quantum-wire superlattice

H. L. Cui and N. J. M. Horing
Department of Physics and Engineering Physics, Stevens Institute of Technology, Hoboken, New Jersey 07030
(Received 14 November 1988; revised manuscript received 13 March 1989)

The dynamical current response of a multiple-quantum-wire superlattice to a time-oscillatory external electric field is examined using Kubo's linear-response theory. Couplings of the quasi-one-dimensional electron gases with phonons (polar optic, and acoustic deformation potential) are discussed to lowest order in terms of a current-current correlation function which embodies both intrawire and interwire electron-electron Coulomb interactions. The associated dynamic screening of the electron-phonon interaction is approximated by employing the random-phase-approximation density-density correlation function for the interacting electrons of the quantum-wire superlattice. The frequency-dependent conductivity of this system is evaluated numerically, exhibiting its variations with temperature and geometrical superlattice parameters.

I. MODEL

In a quasi-one-dimensional electronic system, the motion of the conduction electrons is quantized in two directions, say x and y, while they move freely in the z direction. The quantum-wire superlattice which we consider is composed of an infinite periodic two-dimensional array of such quasi-one-dimensional (quasi-1D) electronic conductors, with all the wires parallel to the z direction. Recent studies of such systems have explored their electronic response,[1,2] collective excitations,[3] as well as linear[4] and hot-electron transport[5] properties. In this paper, our interest is focused on the high-frequency transport of a multiple-quantum-wire superlattice. Our treatment in terms of Kubo linear-response theory for dynamic perturbations is equivalent to the memory-function approach and the balance-equation approach, all of which have been employed recently in the analysis of high-frequency conduction for quasi-2D heterostructures and superlattices,[6-9] and are readily extended to the quasi-1D superlattice.

We consider an infinite 2D array of cylindrical wires along the z direction, with complete confinement of electronic motion within the cylindrical quantum wells (linear electron density n_0), neglecting tunneling of the electrons between the wires. However, electrons on different wires interact via their Coulomb potential, as do electrons within a given wire. Transport of electrons under an applied electric field $\mathbf{E}(t)=\hat{\mathbf{z}}E_0\exp(-i\omega t)$ is limited by electron-phonon scattering which is dynamically screened by the 1D electron-gas superlattice. We assume that the electrons occupy the lowest subband only, which is parabolic with effective mass m and charge e. Furthermore, we neglect the difference of the background dielectric constant in the quantum wells from that of adjoining regions, so that image potential contributions are ignored.

II. WAVE FUNCTION AND HAMILTONIAN

The quantum wires of radius r_0, are centered at the 2D lattice sites $\bar{R}=n_1a\hat{\mathbf{x}}+n_2b\hat{\mathbf{y}}$ for a rectangular 2D lattice (n_1,n_2 are integers). We take the electronic wave function to have the form (L is a normalization length; also $\hbar=k_B=1$ here)

$$\phi_{\bar{R}k_z\sigma}(\bar{r},z)=L^{-1/2}e^{ik_zz}\zeta(\bar{r}-\bar{R})\ , \tag{1}$$

where $\zeta(\bar{r})=0$ outside the wire $r>r_0$. Note that 2D vectors are designated by overhead bars, $\bar{r}=(x,y)$ and $r=|\bar{r}|$, while 3D vectors are decomposed as $\mathbf{r}=(\bar{r},z)$, with $|\mathbf{r}|=(r^2+z^2)^{1/2}$. The energy eigenvalues corresponding to the eigenstates of (1) are

$$\varepsilon_{k_z}=k_z^2/2m+\varepsilon_0\ . \tag{2}$$

ε_0 denotes the bottom of the lowest subband, which is set to zero henceforth. The unperturbed Hamiltonian in the present model may be written as

$$H=H_e+H_{\rm ph}+H_{e\text{-ph}}\ , \tag{3}$$

where the electronic part is given by

$$H_e=\sum_{\bar{R}}\int d^3r\,\psi^\dagger_{\bar{R}}(\mathbf{r})\left[-\frac{1}{2m}\frac{d^2}{dz^2}\right]\psi_{\bar{R}}(\mathbf{r}) +\tfrac{1}{2}\sum_{\bar{R},\bar{R}'}\int d^3r\int d^3r'\,\psi^\dagger_{\bar{R}}(\mathbf{r})\psi^\dagger_{\bar{R}'}(\mathbf{r}') \times V(\mathbf{r}-\mathbf{r}')\psi_{\bar{R}'}(\mathbf{r}')\psi_{\bar{R}}(\mathbf{r})\ . \tag{4}$$

Expanding the electron field operator $\psi^\dagger_{\bar{R}}(\mathbf{r})$ in the eigenstates of (1), e.g., $\psi^\dagger_{\bar{R}}(\mathbf{r})=\sum_{k_z,\sigma}\phi^*_{\bar{R}k_z\sigma}(\bar{r},z)c^\dagger_{\bar{R}k_z\sigma}$, we obtain

$$H_e=\sum_{\bar{R},k_z,\sigma}\epsilon_{k_z}c^\dagger_{\bar{R}k_z\sigma}c_{\bar{R}k_z\sigma}+\tfrac{1}{2}\sum_{\substack{\bar{R},\bar{R}',\\ k_z,k_z',q_z,\sigma,\sigma'}}V_{\bar{R}\bar{R}'}(q_z)c^\dagger_{\bar{R}k_z+q_z\sigma}c^\dagger_{\bar{R}'k_z'-q_z\sigma'}c_{\bar{R}'k_z'\sigma'}c_{\bar{R}k_z\sigma}\ , \tag{5}$$

where $c^{\dagger}_{\bar{R}k_z\sigma}$ ($c_{\bar{R}k_z\sigma}$) is the creation (destruction) operator for an electron with wave number k_z, spin σ, on the quantum wire centered at lattice site $\bar{R}$. The matrix element of the electron-electron Coulomb potential in (5) is given by

$$V_{\bar{R}\,\bar{R}'}(q_z)=\left[\frac{2e^2}{\kappa}\right]\int d^2r\int d^2r' K_0(q_z|\bar{r}-\bar{r}'|)|\zeta(\bar{r}-\bar{R})|^2|\zeta(\bar{r}'-\bar{R}')|^2 . \tag{6}$$

Here $K_0(q_z|\bar{r}-\bar{r}'|)$ is the zeroth-order modified Bessel function of the second kind, which is characteristic of the one-dimensional Fourier transform of the electron-electron Coulomb interaction potential. κ is the background dielectric constant.

$H_{\rm ph}$ in (3) is the free-phonon Hamiltonian of the bulk system, which we take in the 3D plane-wave representation, wave vector $\mathbf{q}$, branch index λ, and frequency $\Omega_{\mathbf{q}\lambda}$:

$$H_{\rm ph}=\sum_{\mathbf{q},\lambda}\Omega_{\mathbf{q}\lambda}b^{\dagger}_{\mathbf{q}\lambda}b_{\mathbf{q}\lambda} . \tag{7}$$

$b^{\dagger}_{\mathbf{q}\lambda}$ and $b_{\mathbf{q}\lambda}$ are phonon creation and annihilation operators, respectively. The electron-phonon interaction Hamiltonian $H_{e\text{-ph}}$ in the present case takes the form

$$\begin{aligned}H_{e\text{-ph}}&=\sum_{\bar{R}}\int d^3r\,\psi^{\dagger}_{\bar{R}}(\mathbf{r})\psi_{\bar{R}}(\mathbf{r})\sum_{\mathbf{q},\lambda}M(\mathbf{q},\lambda)e^{-i\mathbf{q}\cdot\mathbf{r}}(b_{\mathbf{q}\lambda}+b^{\dagger}_{-\mathbf{q}\lambda})\\&=\sum_{\mathbf{q},\lambda}M(\mathbf{q},\lambda)I(i\bar{\mathbf{q}})(b_{\mathbf{q}\lambda}+b^{\dagger}_{-\mathbf{q}\lambda})\sum_{\bar{R},k_z,\sigma}c^{\dagger}_{\bar{R},k_z+q_z,\sigma}c_{\bar{R},k_z,\sigma}e^{-i\bar{q}\cdot\bar{R}} ,\end{aligned} \tag{8}$$

where $M(\mathbf{q},\lambda)$ is the electron-phonon coupling matrix element, and $I(i\bar{q})=\int d^2r\,|\zeta(\bar{r})|^2e^{-i\bar{q}\cdot\bar{r}}$ is a form factor associated with the confined motion of the electrons.

III. DYNAMIC CONDUCTIVITY

The frequency-dependent conductivity of Kubo linear-response theory is usually written in the form[10]

$$\sigma(\omega)=in_0e^2/m\omega+i\Pi(\omega)/\omega , \tag{9}$$

and the current-current correlation function $\Pi(\omega)$ is expressed in terms of the equilibrium thermodynamic Green's function

$$\Pi(i\omega_\nu)=-\int_0^{\beta}d\tau\,e^{i\omega_\nu\tau}\langle\mathcal{T}_\tau[j(\tau)j(0)]\rangle , \tag{10}$$

where $\beta=1/T$ is the inverse temperature, and $\mathcal{T}_\tau$ is the imaginary time-ordering operator. Our analysis follows standard procedures,[10] save for the appearance of a form factor associated with the electron confinement to the wires, whence

$$\Pi(i\omega_\mu)=-\frac{e^2}{m^2(i\omega_\mu)^2}\sum_{\mathbf{q},\lambda}|M(\mathbf{q},\lambda)|^2|I(i\bar{q})|^2q_z^2\frac{1}{\beta}\sum_\nu\chi(\mathbf{q},i\omega_\nu)[D^{(0)}(i\omega_\mu-i\omega_\nu)-D^{(0)}(-i\omega_\mu)] . \tag{11}$$

The free-phonon propagator $D^{(0)}(i\omega_\mu)$ is given by

$$D^{(0)}(i\omega_\mu)=-2\Omega_{\mathbf{q}\lambda}/(\omega_\mu^2+\Omega_{\mathbf{q}\lambda}^2) , \tag{12}$$

and $\chi(\mathbf{q},i\omega_\mu)$ is the electron density-density correlation function for the quantum-wire superlattice.[1,2] The frequency summation is performed with the usual contour integral, taking account of the poles of $D^{(0)}(i\omega_\mu-z)$ at $z=i\omega_\mu\pm\Omega_{\mathbf{q}\lambda}$, poles of $D^{(0)}(-z)$ at $z=\pm\Omega_{\mathbf{q}\lambda}$, and the branch cut of $\chi(\mathbf{q},z)$ on the real z axis. Forming the analytic continuation of the resulting expression ($i\omega_\mu\rightarrow\omega+i\delta$), we obtain the retarded current-current correlation function as

$$\begin{aligned}\Pi(\omega)=-\frac{e^2}{m^2\omega^2}\sum_{\mathbf{q},\lambda}|M(\mathbf{q},\lambda)|^2|I(i\bar{q})|^2q_z^2\{&\chi(\mathbf{q},\omega+\Omega_{\mathbf{q}\lambda})[n_B(\Omega_{\mathbf{q}\lambda})-n_B(\omega+\Omega_{\mathbf{q}\lambda})]\\&+\chi(\mathbf{q},\omega-\Omega_{\mathbf{q}\lambda})[n_B(\Omega_{\mathbf{q}\lambda})-n_B(\Omega_{\mathbf{q}\lambda}-\omega)]\} ,\end{aligned} \tag{13}$$

where $n_B(x)=[\exp(x/T)-1]^{-1}$ is the Bose-Einstein statistical factor. The real part of the conductivity is obtained using (9) and (13),

$$\begin{aligned}{\rm Re}\sigma(\omega)=\frac{e^2}{m^2\omega^3}\sum_{\mathbf{q},\lambda}&|M(\mathbf{q},\lambda)|^2|I(i\bar{q})|^2q_z^2\\&\times\{{\rm Im}\chi(\mathbf{q},\Omega_{\mathbf{q}\lambda}+\omega)[n_B(\Omega_{\mathbf{q}\lambda})-n_B(\Omega_{\mathbf{q}\lambda}+\omega)]+{\rm Im}\chi(\mathbf{q},\omega-\Omega_{\mathbf{q}\lambda})[n_B(\Omega_{\mathbf{q}\lambda})-n_B(\Omega_{\mathbf{q}\lambda}-\omega)]\} .\end{aligned} \tag{14}$$

IV. DENSITY-DENSITY CORRELATION FUNCTION

The electron density-density correlation function $\chi(\mathbf{q},\omega)$ for the quantum-wire superlattice under consideration may be expressed in a form which takes advantage of the periodic translational invariance in the transverse plane

$$\chi(\mathbf{q},\omega)=\sum_{\bar{R},\bar{R}'} e^{i\bar{q}\cdot(\bar{R}-\bar{R}')}\chi(\bar{R},\bar{R}',q_z,\omega) , \tag{15}$$

where $\chi(\bar{R},\bar{R}',q_z,\omega)$ is the Fourier transform of the retarded function,

$$\chi(\bar{R},\bar{R}',q_z,t)=-i\Theta(t)\sum_{k_z,k_z',\sigma}\langle[c^{\dagger}_{\bar{R}k_z+q_z\sigma}(t)c_{\bar{R}k_z\sigma}(t),\, c^{\dagger}_{\bar{R}'k_z'-q_z\sigma}(0)c_{\bar{R}'k_z'\sigma}(0)]\rangle . \tag{16}$$

The average $\langle\ \rangle$ here is that of the equilibrium ensemble for the interacting electrons characterized by the Hamiltonian H_e, at temperature T. [$\Theta(t)$ is the Heaviside unit step function.] In the absence of Coulomb interaction only those electrons on the same wire contribute to the density-density correlation function in accordance with

$$\chi(\bar{R},\bar{R}',q_z,\omega)=\delta_{\bar{R}\bar{R}'}\chi^{(0)}(q_z,\omega) , \tag{17}$$

where the 1D noninteracting density-density correlation function is

$$\chi^{(0)}(q_z,\omega)=\sum_{k_z,\sigma}\frac{[f(\varepsilon_{k_z+q_z})-f(\varepsilon_{k_z})]}{(\omega+\varepsilon_{k_z+q_z}-\varepsilon_{k_z}+i\delta)} , \tag{18}$$

where $f(\varepsilon)=\{\exp[(\varepsilon-\mu)/T]+1\}^{-1}$ is the Fermi-Dirac distribution function, and μ is the chemical potential, which is determined at a given temperature by its relation to the fixed electron line density $n_0=\sum_{k_z,\sigma}f(\varepsilon_{k_z})$.

Both intrawire and interwire electron-electron interactions can be easily incorporated in the random-phase approximation (RPA). The RPA integral equation for $\chi(\bar{R},\bar{R}',q_z,\omega)$ is given by

$$\chi(\bar{R},\bar{R}',q_z,\omega)=\delta_{\bar{R}\bar{R}'}\chi^{(0)}(q_z,\omega)+\chi^{(0)}(q_z,\omega)\times\sum_{\bar{R}''}V_{\bar{R}\bar{R}''}(q_z)\chi(\bar{R}'',\bar{R}',q_z,\omega) . \tag{19}$$

Here, $V_{\bar{R}\bar{R}'}(q_z)$ is the matrix element of the Coulomb potential given in Eq. (6). Taking advantage of the periodic translational invariance of the infinite two-dimensional lattice $\bar{R}$, and noticing that quantities such as $\chi(\bar{R},\bar{R}',q_z,\omega)$ and $V_{\bar{R}\bar{R}'}(q_z)$ must have the form $\chi(\bar{R}-\bar{R}'q_z,\omega)$ and $V_{\bar{R}-\bar{R}'}(q_z)$ for positional arguments on the wires, one may Fourier transform (19) in the transverse plane $\bar{R}-\bar{R}'\rightarrow\bar{q}$ to achieve an algebraic equation which is readily solved as

$$\chi(\bar{q},q_z,\omega)=\chi^{(0)}(q_z,\omega)/[1-V(\bar{q},q_z)\chi^{(0)}(q_z,\omega)] . \tag{20}$$

The Fourier coefficients in (20) are defined for an arbitrary function $g(\bar{R})$, as $g(\bar{R})=(1/N)\sum_{\bar{q}}g(\bar{q})e^{i\bar{q}\cdot\bar{R}}$, where N is the total number of lattice points, equal to the total number of wires. Thus $V(\bar{q},q_z)$ is given by the inverse Fourier transform of (6), $V(\bar{q},q_z)=\sum_{\bar{R}}V_{\bar{R}0}(q_z)\exp(-i\bar{q}\cdot\bar{R})$. As an alternative to this direct lattice sum, $V(\bar{q},q_z)$ can also be expressed as the sum over reciprocal lattice vectors $\bar{G}$ in the form[1,2] (A_c is the area of the unit cell)

$$V(\bar{q},q_z)=(4\pi e^2/\kappa A_c)\sum_{\bar{G}}\frac{|I(i\bar{q}+i\bar{G})|^2}{[(\bar{q}+\bar{G})^2+q_z^2]} . \tag{21}$$

This expression is more convenient for our present purpose, since it involves the form factor $I(i\bar{q}+i\bar{G})$, and bears some resemblance to the Fourier coefficient of the 3D Coulomb potential.

V. CALCULATIONAL CONSIDERATIONS AND DISCUSSION

In order to bring the formulation above to bear on specific conductivity calculations, it is necessary to specify the transverse envelope wave function $\zeta(\bar{r})$ and its associated form factor $I(i\bar{q})$. For our model of a cylindrical quantum well with infinite barrier wall, the solution of the Schrödinger equation is a Bessel function: $\zeta(\bar{r})=(1.92/\sqrt{\pi r_0})J_0(2.4r/r_0)$ when $r<r_0$, and $\zeta(\bar{r})=0$ otherwise. The corresponding form factor is

$$I(i\bar{q})=7.37\int_0^1 dx\, x[J_0(2.4x)]^2J_0(qr_0x) . \tag{22}$$

As an alternative, one may approximate the envelope wave function by a Gaussian: $\zeta(\bar{r})=(\pi r_0^2)^{-1/2}\exp(-r^2/2r_0^2)$, provided r/r_0 is small, and then the form factor takes the simple form[1]

$$I(i\bar{q})=\exp(-q^2r_0^2/4) . \tag{23}$$

This expression describes Eq. (22) quite well, particularly for small values of qr_0. Both (22) and (23) give the value 1 for $qr_0=0$; however, for large values of qr_0, (23) falls off to zero faster than (22). In our numerical calculations we use the Gaussian approximation which leads to [$I_0(x)$ is the modified Bessel function of the first kind]

$$V_{\bar{R}0}(q_z)=(2e^2/\kappa r_0^2)\exp(-R^2/2r_0^2)\times\int_0^{\infty}dr\, r\exp(-r^2/2r_0^2)K_0(qr)I_0(Rr/r_0^2) . \tag{24}$$

Using Eqs. (14), (20), (23), and (24), we evaluated the real part of the high-frequency conductivity employing

the temperature-dependent density-density correlation function $\chi^{(0)}(q_z,\omega)$ as given by Eq. (18) in Eq. (20) along with the self-consistently determined chemical potential $\mu=\mu(T,n_0)$. For scattering mechanisms, the electrons are taken to interact with longitudinal polar optic phonons through Fröhlich coupling $|M(\mathbf{q},l)|^2=(2\pi e^2/|\mathbf{q}|)(1/\kappa_\infty-1/\kappa)\Omega_0$, and they interact with acoustic phonons with longitudinal deformation potential coupling $|M(\mathbf{q},l)|^2=\Theta^2|\mathbf{q}|/2dv_{sl}$, with $\Omega_{q\lambda}=|\mathbf{q}|v_{sl}$. Here κ_∞ is the optical dielectric constant, κ the static dielectric constant, Θ the deformation potential, d the mass density of the lattice, and v_{sl} the longitudinal sound velocity. For polar optic phonons we consider $\Omega_{q\lambda}=\Omega_0$ to be a constant. Numerical values of the above quantities are taken here to be those pertaining to a bulk GaAs semiconductor, $\kappa_\infty=10.8$, $\kappa=12.9$, $\Omega_0=35.4$ meV, $\Theta=8.5$ eV, $d=5.31$ g/cm^3, $v_{sl}=5.29\times10^3$ m/s, electron effective mass $m=0.07m_0$ (m_0 is the free-electron mass), and the electron density used is $n_0=1\times10^8$ m^{-1} per wire. For simplicity we only consider a 2D square lattice with lattice constant a. Our numerical calculations are focused on the inverse relaxation time $\tau^{-1}(\omega)$ rather than $\mathrm{Re}\sigma(\omega)$. Within the framework of this high-frequency analysis, they are related simply as $1/\tau(\omega)=(m\omega^2/n_0e^2)\mathrm{Re}\sigma(\omega)$. Within the Born approximation for scattering interactions, contributions to the inverse relaxation time by the various phonon branches are additive and we examine the polar optic phonons and acoustic phonons separately.

In Fig. 1 we plot $\tau^{-1}(\omega)$ due to polar optic phonon scattering as a function of frequency at temperatures $T=20$, 77, 150, and 300 K, with $r_0=50$ Å and $a=150$ Å. Resonant excitations of polar optic phonons by the frequency-dependent external field are evident. At low temperatures the phonon frequency Ω_0 serves as a threshold, below which the inverse relaxation time approaches zero. Note that $1/\tau(\omega)$ does not peak at Ω_0, but rather peaks at a frequency somewhat above Ω_0. This shift toward higher frequency is more pronounced at lower temperature. It seems likely that this indicates a possible mixing of the phonon frequency with a collective electron mode. The latter may be roughly estimated by using the "bulk" plasma frequency for the quantum-wire superlattice at $\omega_p=(4\pi n_0e^2/\kappa ma^2)^{1/2}\simeq0.73\Omega_0$, leading to a coupled mode frequency $(\omega_p^2+\Omega_0^2)^{1/2}\simeq1.2\Omega_0$. The actual plasmon spectrum, however, is more complicated,[2] with plasma frequencies ranging continuously from the above-mentioned 3D plasma frequency for wave vectors parallel to the axes of the wires, to zero for wave vectors perpendicular to the axes of the wires, neglecting higher subband excitations.[11] In the absence of phonon scatterings superlattice plasmons alone contribute a broad maximum, centered about ω_p, in the optical-absorption spectrum.[2] It is reasonable, therefore, to expect that any mixing of the optical-phonon mode with plasma excitations will primarily involve the bulk plasmon, which is preferentially excited in the close-packing, high-density limit. Similar circumstances in the case of closely packed 2D planar superlattices have been discussed extensively in connection with high-frequency transport.[8,9] Such a close-packed, high-density limit is elusive analytically in the treatment of a multiple-quantum-wire superlattice, due to the singular behavior of the 1D Fourier component of the electron-electron Coulomb potential.[1] However, following earlier work,[1,2] we treat this matter by maintaining a finite wire radius and finite (if small) wire separation numerically.

To investigate the specific role played by the electron-electron interaction, we have recalculated the inverse relaxation time in the absence of all Coulomb interactions (both intrawire and interwire). This is shown in Fig. 2,

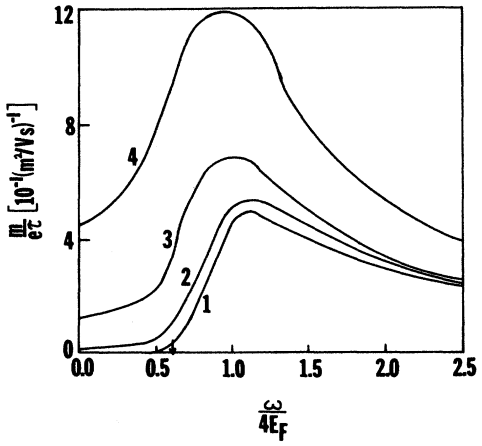

FIG. 1. Plot of $1/\tau(\omega)$ due to polar optic-phonon scattering vs normalized frequency $\omega/4E_F$ at various temperatures. Curve 1, $T=20$ K; curve 2, $T=77$ K; curve 3, $T=150$ K; curve 4, $T=300$ K. Also, $r_0=50$ Å, and $a=150$ Å. The arrow indicates the optic-phonon frequency Ω_0.

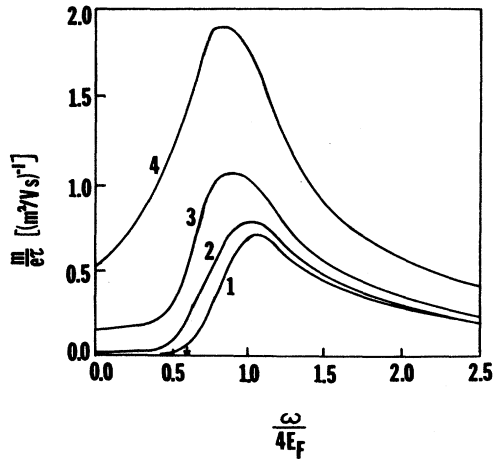

FIG. 2. $1/\tau(\omega)$ due to polar optic-phonon scattering as a function of normalized frequency $\omega/4E_F$, at various temperatures in the absence of Coulomb interactions. Curve 1, $T=20$ K; curve 2, $T=77$ K; curve 3, $T=150$ K; curve 4, $T=300$ K. Also, $r_0=50$ Å and $a=150$ Å. The arrow indicates the position of Ω_0.

where all other parameters are the same as used in obtaining Fig. 1. Compared with Fig. 1, peak values of $1/\tau(\omega)$ are all shifted to lower frequency by about 20%, which is to be expected in conjunction with the discussion above. The absence of screening due to the electron-electron interaction also makes the electron-phonon interaction more effective, and this is reflected in Fig. 2 as $1/\tau(\omega)$ is increased compared with corresponding results in Fig. 1. (All figures except Fig. 2 involve the full complement of electron-electron interactions, both interwire and intrawire.)

We should also point out that, unlike the dc conductivity due to phonon scattering which vanishes for $T=0$, the corresponding high-frequency conductivity due to phonon scattering retains a finite value as the temperature approaches zero, since the high-frequency electric field is capable of exciting lattice vibrations even at $T=0$: However, the driving frequency has to exceed the phonon frequency, as can be seen from the zero-temperature limit of Eq. (14):

$$\mathrm{Re}\sigma(\omega)=(e^2/m^2\omega^3)\sum_{\mathbf{q},\lambda}|M(\mathbf{q},\lambda)|^2\,|I(i\bar{q})|^2\,q_z^2 \times \mathrm{Im}\chi(\mathbf{q},\omega-\Omega_{q\lambda})\Theta(\omega-\Omega_{q\lambda})\ . \tag{25}$$

At higher temperatures the phonon frequency ceases to be a threshold, as seen in Figs. 1 and 2, due to the presence of thermally excited phonons.

In Fig. 3 we exhibit the acoustic-phonon contribution to the inverse relaxation time as a function of frequency, at temperatures $T=20$, 77, 150, and 300 K, with the same geometrical parameters. Comparison with Fig. 1 shows that the acoustic-phonon scattering is always less effective than optic-phonon scattering, being an order of magnitude smaller. Since the acoustic-phonon spectrum

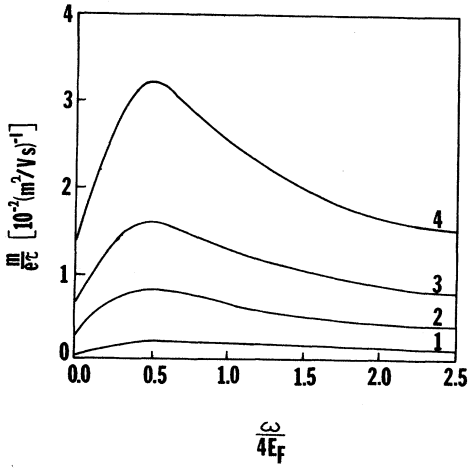

FIG. 3. Plot of $1/\tau(\omega)$ due to acoustic-phonon scattering as a function of normalized frequency $\omega/4E_F$, at various temperatures. Curve 1, $T=20$ K; curve 2, $T=77$ K; curve 3, $T=150$ K; curve 4, $T=300$ K. $r_0=50$ Å and $a=150$ Å.

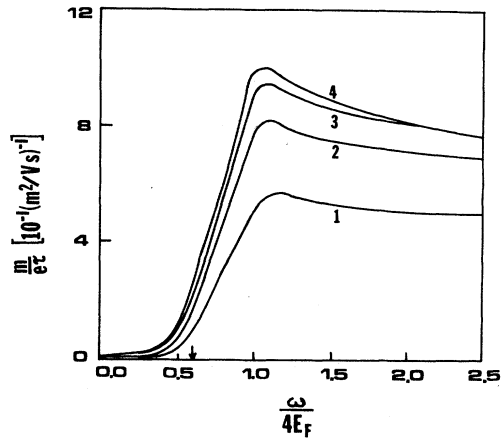

FIG. 4. Plot of $1/\tau(\omega)$ vs $\omega/4E_F$ for polar optic-phonon scattering for various values of quantum-wire separation a. $T=77$ K and $r_0=20$ Å. Curve 1, $a=40$ Å; curve 2, $a=60$ Å; curve 3, $a=100$ Å; curve 4, $a=200$ Å. The arrow marks the position of Ω_0.

extends to low frequencies $\Omega_{q,\lambda}=v_{sl}|\mathbf{q}|$, it also lacks the threshold character associated with optical-phonon scattering. Maximum values of $1/\tau(\omega)$ in Fig. 3 can again be attributed to the collective electron modes, since $\omega_p/4E_F\simeq 0.5$ corresponds closely to the maxima in $1/\tau(\omega)$.

We have also examined the influence of geometrical parameters (the wire radius r_0 and the lattice constant a) on the inverse relaxation time. The results are exhibited in Figs. 4 and 5. In Fig. 4 we show the inverse relaxation time due to optical-phonon scattering versus frequency for a fixed temperature $T=77$ K and wire radius $r_0=20$ Å, with varying lattice constant $a=40$, 60, 100, and 200

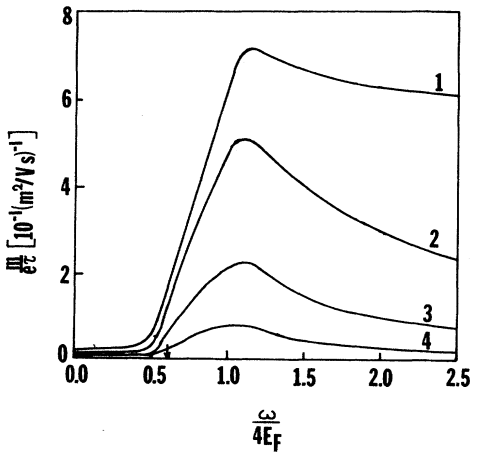

FIG. 5. Plot of $1/\tau(\omega)$ vs $\omega/4E_F$ for polar optic-phonon scattering for various superlattice geometrical parameters r_0 and a, at $T=77$ K. Curve 1, $r_0=20$ Å and $a=50$ Å; curve 2, $r_0=50$ Å and $a=150$ Å; curve 3, $r_0=100$ Å and $a=250$ Å; curve 4, $r_0=200$ Å and $a=500$ Å. The arrow marks the position of Ω_0.

Å. Transition from the near-bulk close-packed limit to the single-wire limit is clearly shown. With $a-40$ Å and $r_0=20$ Å, the superlattice resembles a bulk material, whose optical conductivity is similar to its counterpart in a bulk semiconductor.[12] On the other hand, at $r_0=20$ Å and $a=200$ Å, we can safely say that the system is in the single-wire limit, and $1/\tau(\omega)$ corresponds to the inverse relaxation time for a single quantum wire, with intrawire Coulomb interaction. It is also of interest to study the dependence of the high-frequency conductivity upon the radius of the wire. This is shown in Fig. 5, where $1/\tau(\omega)$ is plotted as a function of frequency, for a fixed temperature $T=77$ K. The set of parameters r_0 and a are changed in about the same proportion: $r_0=20$ Å, $a=50$ Å; $r_0=50$ Å, $a=150$ Å; $r_0=100$ Å, $a=250$ Å; $r_0=200$ Å, $a=500$ Å. Two effects are in evidence as r_0 becomes larger while keeping r_0/a fixed: (1) the inverse relaxation time decreases, and (2) the maximum value of $1/\tau(\omega)$ moves toward lower frequency. The first effect is mainly a consequence of the presence of the form factor $|I(i\bar{q})|^2$ in the expression of the conductivity, which becomes exponentially smaller as r_0 is increased. The shift of the maximum value of $1/\tau(\omega)$ toward lower frequency is primarily due to the increase of the lattice constant a, leading to a reduced plasma frequency ω_p (increasing a is equivalent to decreasing the bulk carrier density).

In conclusion, we have calculated the high-frequency conductivity for a multiple-quantum-wire superlattice, treating phonon scattering in the Born approximation. The electron-electron interaction (both intrawire and interwire) is fully incorporated within the random-phase approximation, which serves to screen the electron-phonon interaction dynamically. The results of our numerical evaluation of the frequency-dependent inverse relaxation time exhibit threshold and resonance behavior, which we have interpreted in terms of coupled optic-phonon–plasmon excitations for the quantum-wire superlattice. Our examination includes various temperatures, and superlattice geometrical parameters, such as the radius of the wire and the separation between wires. The limits of nearly bulk behavior and single-wire behavior are clearly exhibited upon varying the geometrical parameters. It is also shown that acoustic-phonon scattering is always less effective (by a factor of ~ 10) than optical-phonon scattering at all temperatures considered. Finally, we should point out that, in the present treatment, occupation of higher subbands and the associated intersubband transitions[13] are neglected. Another simplification employed is the infinite barrier cylindrical potential-well model. As information about the confinement and subband structure of quasi-one-dimensional semiconductor quantum-wire superlattices is further developed, the present study should be refined to address these points.

ACKNOWLEDGMENTS

The authors wish to acknowledge support of the John von Neumann National Supercomputer Center, Princeton, New Jersey in providing computing resources.

[1]M. M. Mohan and A. Griffin, Phys. Rev. B **32**, 2030 (1985); A. Griffin and G. Gumbs, Phys. Rev. B **36**, 9275 (1987); G. Gumbs and X. D. Zhu, Solid State Commun. (to be published).

[2]P. F. Williams and A. N. Bloch, Phys. Rev. B **10**, 1097 (1974).

[3]W. M. Que and A. Kirczenow, Phys. Rev. B **37**, 7153 (1988).

[4]S. Das Sarma and X. C. Xie, Phys. Rev. B **35**, 9875 (1987).

[5]D. Chattopadhyay and A. Bhattacharyya, Phys. Rev. B **37**, 7105 (1988).

[6]N. Tzoar and C. Zhang, Phys. Rev. B **32**, 1146 (1985).

[7]N. Tzoar and C. Zhang, Phys. Rev. B **33**, 2642 (1986).

[8]X. L. Lei, N. J. M. Horing, and J. Q. Zhang, Phys. Rev. B **33**, 2912 (1986); **34**, 1139 (1986); **35**, 2834 (1987).

[9]X. L. Lei, H. L. Cui, and N. J. M. Horing, Phys. Rev. B **38**, 8230 (1988).

[10]G. D. Mahan, *Many-Particle Physics* (Plenum, New York, 1981).

[11]See Ref. 3 for a discussion of the intersubband plasma excitations.

[12]R. Sirko and D. L. Mills, Phys. Rev. B **18**, 4373 (1978).

[13]X. G. Wu, Phys. Rev. B **39**, 8062 (1989).